

RESEARCH

Open Access



Development of a portable hypoxia chamber for ultra-high dose rate laser-driven proton radiobiology applications

Pankaj Chaudhary^{1,2*} , Deborah C. Gwynne², Boris Odlozilik^{2,8}, Aaron McMurray², Giuliana Milluzzo^{2,7}, Carla Maiorino¹, Domenico Doria^{2,3}, Hamad Ahmed^{2,5}, Lorenzo Romagnani⁴, Aaron Alejo², Hersimerjit Padda⁶, James Green⁵, David Carroll⁵, Nicola Booth⁵, Paul McKenna⁶, Satyabrata Kar², Giada Petringa⁷, Roberto Catalano⁷, Francesco P. Cammarata⁷, Giuseppe A. P. Cirrone⁷, Stephen J. McMahon¹, Kevin M. Prise^{1*} and Marco Borghesi^{2*}

Abstract

Background: There is currently significant interest in assessing the role of oxygen in the radiobiological effects at ultra-high dose rates. Oxygen modulation is postulated to play a role in the enhanced sparing effect observed in FLASH radiotherapy, where particles are delivered at 40–1000 Gy/s. Furthermore, the development of laser-driven accelerators now enables radiobiology experiments in extreme regimes where dose rates can exceed 10⁹ Gy/s, and predicted oxygen depletion effects on cellular response can be tested. Access to appropriate experimental environments, allowing measurements under controlled oxygenation conditions, is a key requirement for these studies. We report on the development and application of a bespoke portable hypoxia chamber specifically designed for experiments employing laser-driven sources, but also suitable for comparator studies under FLASH and conventional irradiation conditions.

Materials and methods: We used oxygen concentration measurements to test the induction of hypoxia and the maintenance capacity of the chambers. Cellular hypoxia induction was verified using hypoxia inducible factor-1 α immunostaining. Calibrated radiochromic films and GEANT-4 simulations verified the dosimetry variations inside and outside the chambers. We irradiated hypoxic human skin fibroblasts (AG01522B) cells with laser-driven protons, conventional protons and reference 225 kVp X-rays to quantify DNA DSB damage and repair under hypoxia. We further measured the oxygen enhancement ratio for cell survival after X-ray exposure in normal fibroblast and radioresistant patient-derived GBM stem cells.

Results: Oxygen measurements showed that our chambers maintained a radiobiological hypoxic environment for at least 45 min and pathological hypoxia for up to 24 h after disconnecting the chambers from the gas supply. We observed a significant reduction in the 53BP1 foci induced by laser-driven protons, conventional protons and X-rays in the hypoxic cells compared to normoxic cells at 30 min post-irradiation. Under hypoxic irradiations, the Laser-driven

*Correspondence: p.chaudhary@qub.ac.uk; k.prise@qub.ac.uk; M.Borghesi@qub.ac.uk

¹ The Patrick G. Johnston Centre for Cancer Research, Queen's University Belfast, Lisburn Road, Belfast BT9 7AE, Northern Ireland, UK

² Centre for Plasma Physics, School of Mathematics and Physics, Queen's University Belfast, Belfast BT7 1NN, Northern Ireland, UK

Full list of author information is available at the end of the article



© The Author(s) 2022. **Open Access** This article is licensed under a Creative Commons Attribution 4.0 International License, which permits use, sharing, adaptation, distribution and reproduction in any medium or format, as long as you give appropriate credit to the original author(s) and the source, provide a link to the Creative Commons licence, and indicate if changes were made. The images or other third party material in this article are included in the article's Creative Commons licence, unless indicated otherwise in a credit line to the material. If material is not included in the article's Creative Commons licence and your intended use is not permitted by statutory regulation or exceeds the permitted use, you will need to obtain permission directly from the copyright holder. To view a copy of this licence, visit <http://creativecommons.org/licenses/by/4.0/>. The Creative Commons Public Domain Dedication waiver (<http://creativecommons.org/publicdomain/zero/1.0/>) applies to the data made available in this article, unless otherwise stated in a credit line to the data.

protons induced significant residual DNA DSB damage in hypoxic AG01522B cells compared to the conventional dose rate protons suggesting an important impact of these extremely high dose-rate exposures. We obtained an oxygen enhancement ratio (OER) of 2.1 ± 0.1 and 2.5 ± 0.1 respectively for the AG01522B and patient-derived GBM stem cells for X-ray irradiation using our hypoxia chambers.

Conclusion: We demonstrated the design and application of portable hypoxia chambers for studying cellular radiobiological endpoints after exposure to laser-driven protons at ultra-high dose, conventional protons and X-rays. Suitable levels of reduced oxygen concentration could be maintained in the absence of external gassing to quantify hypoxic effects. The data obtained provided indication of an enhanced residual DNA DSB damage under hypoxic conditions at ultra-high dose rate compared to the conventional protons or X-rays.

Keywords: Ultra-high dose rate, Laser-driven protons, Hypoxia, DNA repair

Background

It has been known for many years that oxygen is a key radiation sensitiser and in the absence of oxygen significant radioresistance occurs which limits the effectiveness of radiotherapy [1]. Importantly, with increasing linear energy transfer (LET) the radiosensitisation by oxygen reduces even for light ions such as protons [2, 3]. Ion beam therapy using high linear energy transfer (LET) particles is recognised as an effective approach for killing radioresistant and hypoxic tumour cells [4–6]. Charged particles also provide normal tissue sparing which has enabled dose escalation for better tumour control [7–9]. Recent studies, with low LET electrons, have shown that high dose-rate approaches such as FLASH radiotherapy (typically > 100 Gy/s) are promising due to the therapeutic index boost they provide through an enhanced normal tissue sparing [10]. While the majority of the FLASH studies have used electrons, protons have also been demonstrated to be effective in sparing the normal tissues at FLASH dose rates [11] and can potentially treat deep seated tumours which is not currently feasible with FLASH electrons. FLASH results have led to a renewed interest in the radiobiological effects at high dose rates, and emerging particle sources provide today opportunities for irradiating samples at dose rates much higher than currently used in FLASH. Ultra-high dose rates (UHDR) in the range of 10^9 – 10^{10} Gy/s have already been achieved by using laser-driven proton accelerators [12–15]. While most of the cellular effects at UHDR are still unknown, some effects on the DNA damage and repair have been reported including our own studies [16, 17]. A role for Oxygen depletion at high dose rates was first suggested about 50 years ago [18] and recently a number of studies have also suggested that oxygen concentration during irradiation may affect the radiobiological outcome and often result in normal tissue sparing [18–22]. A recent modelling study by Petersson et al. [23] using FLASH electrons suggested that cellular protective effects of FLASH irradiation may not be observed

at atmospheric oxygen tension level as doses as high as 10–100 s Gy would be needed to deplete the significant levels of oxygen.

While studies have been performed with FLASH electrons under various oxygenation conditions [22, 24], information on the radiobiological effects of protons under hypoxia is still limited [25–28] and there are no reports at FLASH and ultra-high dose rates. This could mainly be attributed to the lack of suitable experimental systems, including appropriate hypoxia chambers, enabling such experiments with a variety of radiation sources where constraints related to physical ion beam parameters and cellular physiology make measurements difficult.

Several groups have developed hypoxia chambers for radiobiology studies but most of these chambers can be used successfully only in a horizontal orientation when placed on flat surfaces [26, 29, 30]. However, most of the experimental fixed beamlines in the cyclotron research facilities, as well as the beams produced by high power lasers within laser interaction chambers, have a horizontal orientation that allows cells irradiation only in a vertical position i.e. perpendicular to the beam. In this situation, horizontal chambers may not be suitable as there is a high chance of liquid medium spillage and mixing when multi-well plates or petri-dishes are used. The permanent mounting of hypoxia incubators on a beam line is impractical in many situations due to dosimetry requirements, and a simple lightweight, gas-impermeable, portable chamber capable of maintaining hypoxic environment for long durations would be beneficial. Most of the hypoxia chambers used previously either relied on continuous hypoxia gas supply during irradiation or gassing before irradiation. Re-oxygenation of the chambers upon disconnecting from the gas supply or over time can significantly impact the radiobiological response, as radiobiological hypoxia oxygen concentration is less than equal to 0.4% oxygen and values above this could be reached rapidly. Metsällä et al. [31] have developed a portable hypoxia chamber equipped with a gas cylinder for controlling multiple samples at a time. Walter et al.

also demonstrated the use of a hypoxia chamber for studies with high energy carbon, oxygen and nitrogen ions [26, 32]. While their hypoxia chamber system was effective for high energy particles, the chamber was not tested for the lower energies of current relevance to laser-driven protons, where the particle energies used for cellular radiobiology endpoints are often typically ~10–20 MeV, with short ranges.

The procedures and constraints of laser driven proton irradiation are currently very different than conventional proton beam irradiations using RF accelerator beams. The workflow in a laser-driven proton irradiation procedure is not as fast as in a conventional proton beam experiment. The proton beam is generated inside a high vacuum laser interaction chamber by focussing very high power lasers onto thin targets. Biological samples cannot be irradiated inside the interaction chamber due to the high vacuum ($<1 \times 10^{-4}$ mbar) so, in a typical set-up [16], the beam needs to be steered out of the interaction chamber using strong magnets, and exits the chamber through a thin plastic window (typically Kapton). This Kapton window acts as a sample irradiation port and is kept isolated from any outside elements by installation of a narrow diameter (20 cm) sample re-entry tube perpendicular to the axis of the exit window. This limits the size of cell samples which can be irradiated and only compact hypoxia chambers can be used to control the gassing conditions. The compact hypoxia chambers are introduced on a rail through this narrow tube such that the hypoxia chamber window can align with the Kapton window during the irradiation. Target alignment and radiation safety checks required before each shot significantly increase the set-up time required to prepare for and complete an irradiation compared to conventional proton exposures. The cells, attached as monolayers in the Mylar dishes, cannot be held in upright position for long durations as this may lead to their dehydration. To overcome this problem, the hypoxia chambers can be mounted on remotely controlled motorized flippers. Immediately before irradiation, the hypoxia chambers are slowly flipped vertically and after irradiation they are returned to the horizontal position, removed and taken for post irradiation processing. We addressed all these issues during the design and development of a portable hypoxia chamber and successfully used it to measure ultra-high dose-rate laser-driven proton DNA damage and repair under oxic and hypoxic conditions alongside comparator studies with conventional dose rate protons and X-rays. Furthermore, we also measured the oxygen enhancement ratio (OER) for survival of radioresistant patient derived Glioblastoma (E2) and normal human skin fibroblast AG01522 cells irradiated with reference X-rays in the hypoxic chambers to validate the radiobiological impact

of irradiating two radiobiologically variable cell lines under hypoxia. Overall, our results clearly indicate the effectiveness of these hypoxia chambers in the maintenance of a hypoxic environment during irradiation with various radiation qualities, without adversely affecting the physical and radiobiological readouts.

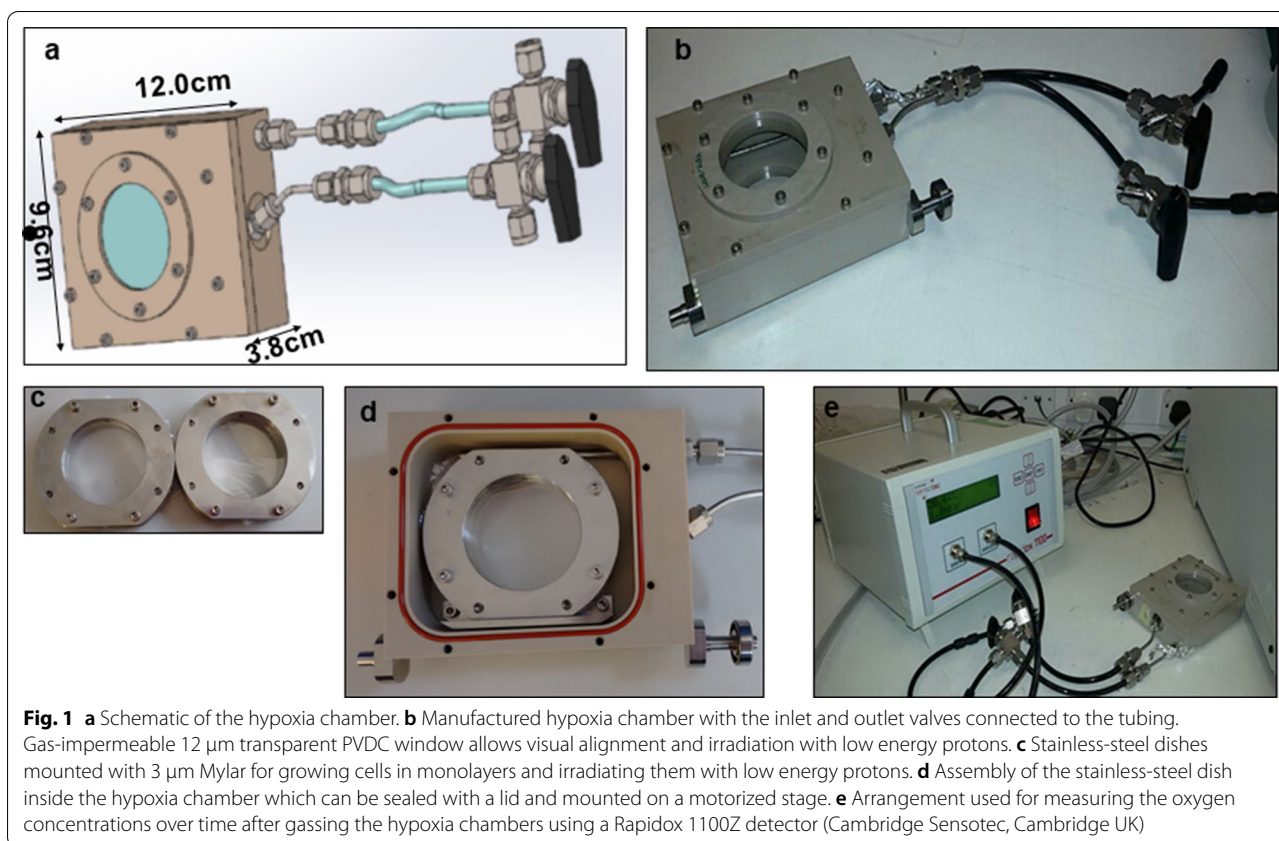
Materials and methods

Cells and culture

Both human cell lines used in this study were authenticated through STR profiling at European Collection of Authenticated Cell Cultures (ECACC) operated by Public Health England, United Kingdom. AG01522B cells were obtained from the Coriell Institute for Medical Research (Camden, New Jersey, USA) and maintained in α -modified Minimum Essential Medium (MEM) (Sigma Aldrich) supplemented with 20% Fetal Bovine Serum (FBS) and 1% penicillin–streptomycin (Thermo Fischer Scientific, Loughborough, UK). These cells were routinely tested for Mycoplasma contamination and have a finite life span. For all our experiments, early passage cells within passage 2–4 after procuring from the Coriell Repository. Glioblastoma stem like cells (E2 cells) were kindly provided by Prof. Anthony Chalmers (University of Glasgow, UK) and have been previously characterized for the expression of stem cell biomarkers such as NG2, Olig2 and Sox-2. These cells are cultured in Advanced Dulbecco's Modified Eagle's Medium/F-12 serum free medium, supplemented with B27, N2, L-Glutamine, heparin, epidermal growth factor and basal fibroblast growth factor (Thermo Fischer Scientific, Loughborough, UK) and were also routinely tested for mycoplasma contamination. Cell culture flasks and cell dishes used for E2 cells were coated with a thin layer of growth factor reduced basement membrane Matrigel (Corning, NY, USA) dissolved in DMEM/F-12 medium at a dilution of 1:40 giving a final concentration of matrigel proteins of 0.225 mg/ml of medium. All the cells were maintained in 5% CO₂ with 95% humidity at 37 °C.

Hypoxia chamber design, hypoxia induction and Oxygen measurement

The design and assembly of the hypoxia chamber is shown in Fig. 1a–e. The main body of the hypoxia chamber is a hollow box made of polyetheretherketone (PEEK) (Direct Plastics, Sheffield, England, UK) sheet of 5 mm with dimensions of 12.0 cm (length) 9.6 cm (width) and 3.8 cm (height). The front and rear faces of the chamber have 4.7 cm diameter circular openings. These openings are sealed with a 12.5 μ m oxygen impermeable polyvinylidene chloride (PVDC) or Saran membrane (Goodfellow Cambridge Ltd, Huntingdon, England), attached with 0.4 cm and 0.2 cm thick PEEK rings screwed with



silicone ‘O’ rings underneath for sealing on both the front and rear, creating two transparent windows. Two stainless steel gas ports, one inlet and one outlet, were attached to the right side of the box. These ports were connected to two-way valves with flexible polyurethane tubing. The inlet port extends inside the chamber to the left-hand side of the box to ensure uniform thorough saturation of the chamber with a hypoxia gas mixture.

Oxygen concentration measurements were taken for six independent chambers using an oxygen gas analyser (Rapidox 1100Z, Cambridge Sensotec, Cambridge UK) connected to the chambers in the arrangement shown in Fig. 1e. Briefly, the chambers were flushed with the hypoxic gas (95% N₂, 5% CO₂, BOC Gases, Belfast, UK), for 15 min through the inlet port. The outlet from the hypoxia chamber was fed into the inlet port of the oxygen analyser and the outlet of the analyser was connected to a small water-filled flask for visual monitoring of the gas flow rate. The chambers were gassed at a flow rate of 0.5–1 L per minute until the oxygen saturation dropped down to 0.005–0.01% between 0 and 3 mm Hg oxygen tension. At this stage, the inlet and outlet valves of the chambers were closed, the oxygen analyser outlet tube was immediately removed from the water-filled flask and attached to the inlet port of the chamber. In this way a

closed loop was formed between the hypoxia chamber and the oxygen gas analyser that allowed continuous monitoring of the oxygen concentration inside the chamber for the next 24 h.

For hypoxia induction, the cells were grown inside customized stainless steel dishes with a 3 μm Mylar membrane base for cell attachment (Fig. 1c) which was mounted inside the sterile (thoroughly wiped with 70% ethanol and dried in the laminar air flow) chamber (Fig. 1d) in less than 5 min under the sterile air of the laminar flow hood. The whole assembly was then placed in a cell culture incubator at 37 °C where the chambers were continuously gassed for 4 h with the hypoxia gas mixture. To quantify the initial change in oxygen concentration, oxygen concentration data from all chambers were pooled together and fitted using an equation of the form $C = C_0(1 - e^{-kt})$, where C_0 is a plateau concentration and k is a rate constant describing the rate of reoxygenation. The flexible fittings used in the hypoxia chambers make them suitable to connect more than six hypoxia chambers in series easily, the only limitation being the size of the incubator holding the chambers at the optimum temperature for gassing. For larger experiments, one can, in principle, scale up the set up without any technical issues, although combinations using more

than 12 hypoxia chambers may need further verification e.g. to test whether the pressure inside the hypoxia chambers at the beginning or the end of the series is similar or significantly variable.

Irradiations

Laser-driven protons

Laser-driven protons were generated at the Petawatt arm of the VULCAN laser at the Central Laser Facility of the Rutherford Appleton Laboratory, Didcot, Oxford, UK. Protons were accelerated by focussing the Vulcan Laser at an intensity of order $5 \times 10^{20} \text{ W/cm}^2$ onto a 25 μm -thick aluminium foil. The protons were accelerated through the Target Normal Sheath Acceleration mechanism [33, 34] from the hydrogen contained in a contaminant layer on the rear surface of the target. As typical for this mechanism, the energy spectrum of the accelerated protons was broadband, approximately decreasing exponentially, up to a cut-off energy of $\sim 30 \text{ MeV}$. The proton irradiation setup was designed to minimize the distance between the target and the cells, compatibly with energy selection and shielding requirements, in order to achieve a suitable dose on the cells on a single-shot basis, as well as to minimize the temporal duration of the ion irradiation. A 1.0 T magnet was used in conjunction with a collimator and pinhole to disperse and spatially select the proton energy and irradiate the cells with the selected $15 \pm 1 \text{ MeV}$ protons. The protons exited the interaction chamber through a flange-mounted 50 μm Kapton window before reaching the cells, located approximately 30 cm away from the laser interaction point at the transverse position corresponding to the 15 MeV proton spatial dispersion. Dose rates of $2 \times 10^9 \text{ Gy/s}$ were achieved in single ion pulses of $\sim 400 \text{ ps}$ duration. Hypoxia chambers with motorised mounts were inserted on a slide rail through a re-entrant tube in a horizontal position to keep the cells submerged in liquid medium. Just prior to firing the laser, the hypoxia chambers were raised slowly from the horizontal to vertical position, so that the cells, without any cell culture medium layer in front, were precisely located in the beam path, through a remotely controlled motorized mount as shown in Fig. 2a–c.

Conventional dose rate protons

Cells were irradiated at a conventional dose rate of 4 Gy per minute with the proton beams accelerated by the superconducting cyclotron (CS) along the CATANA proton therapy beam line of Laboratory Nazionale del Sud (LNS), Istituto Nazionale Fisica Nucleare (INFN) Catania, Italy. The 30 MeV proton beam extracted from the CS, was then degraded using a 4 mm-thick PMMA range shifter placed in-air along the beam line, in order to obtain 15 MeV protons at the cell position. The portable

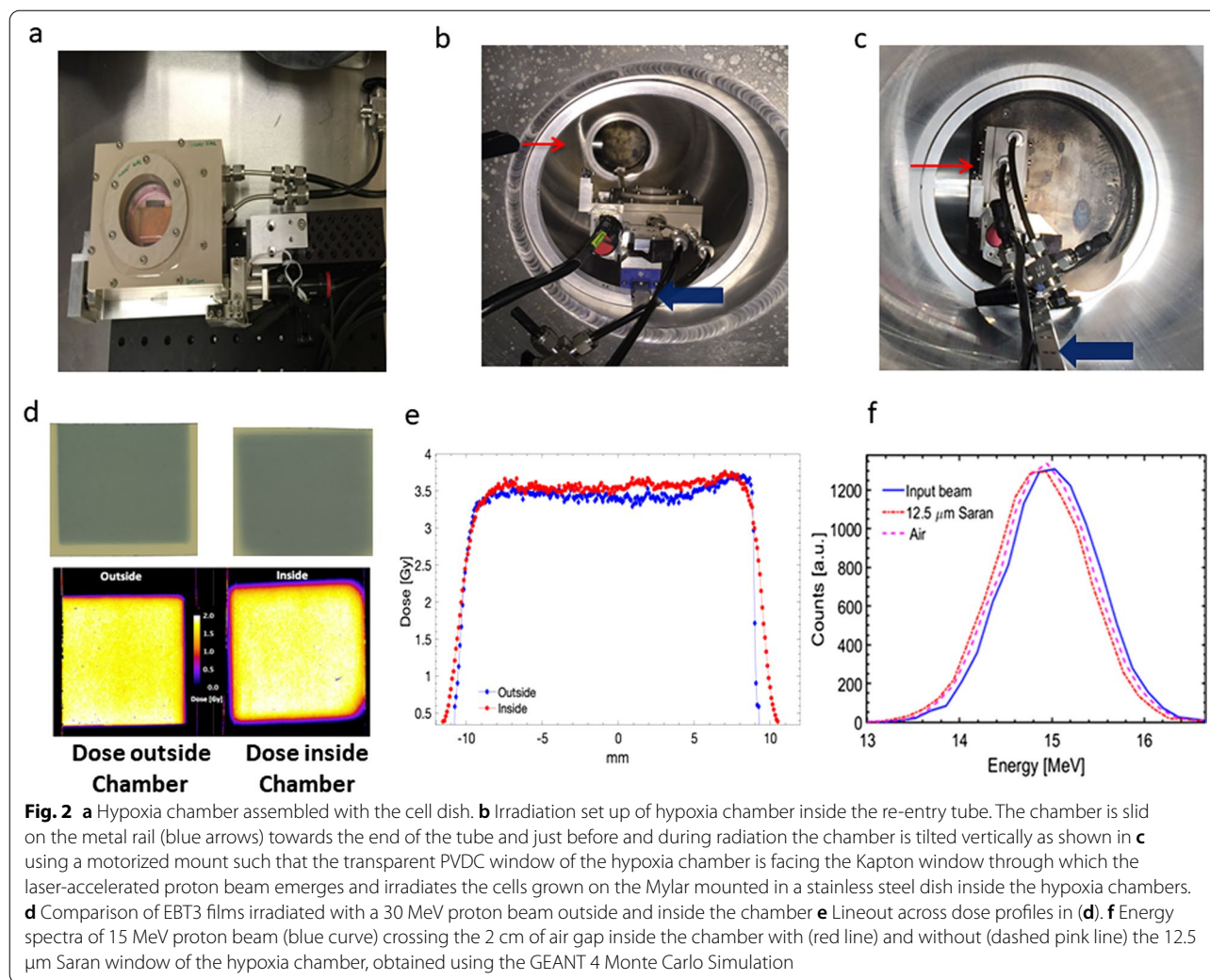
hypoxia chambers were mounted inside the Perspex sample holder and aligned on a motorized X–Y translator stage as shown in supplementary figure-1, and movement across X and Y axis was controlled remotely. A 2 cm \times 2 cm collimated proton beam irradiated the cells inside the hypoxia chambers and nine collimated fields were used to fully irradiate the cell dish.

X-rays

Cellular irradiations with 225 kVp X-rays were performed in house in our institution using a X-Rad 225 (Precision X-ray, Connecticut, USA), X-ray generator at a dose rate of 0.59 Gy/min. Both hypoxic and normoxic cells were irradiated inside the shielded cabinet for the time duration required to deliver each dose.

Dosimetry and simulations for hypoxia chambers

Before irradiating the cells, we first performed dosimetry inside and outside the blank hypoxia chambers using EBT3 Radiochromic films, which are known to show a dose-rate independence for dose rates as high as 10^{10} Gy/s [35, 36], to test for any dose variations (shown in Fig. 2d, e). The horizontal dose profiles measured with the EBT3 film placed at the cell position inside the chamber (red data points) and outside the chamber (blue data points) are shown in Fig. 2e for comparison. During the cellular irradiations employing laser-driven protons, the dose delivered to the cells placed within the hypoxia chamber was measured, for every irradiation, using EBT3 type films placed just after the dish, i.e. behind the 3 μm Mylar foil where the cells were attached. This setup allowed measurement of the dose in a position very close to the position of the cells. The EBT3 Radiochromic films had been previously calibrated with a 35 MeV clinical proton beam conventionally accelerated at the CATANA beam line of the LNS-INFN. Using the dose calibration, and exploiting the demonstrated dose-independence and high spatial resolution of EBT3, it was then possible to reconstruct the absolute dose delivered per shot with a 10% uncertainty at any point of the irradiated region of the cell dish. A Monte Carlo GEANT4 simulation was also performed to estimate the proton energy loss through all the components traversed within the hypoxia chamber, considering as the input a narrow band 15 MeV proton beam impinging into the 12.5 μm PVDC Saran window. The energy loss is not significant as shown in Fig. 2f. We also used EBT3 films for dosimetry of X-rays, which we mainly used to irradiate the cells for cell survival and oxygen enhancement ratio studies as shown in the Additional file 1: Fig. S1. As X-rays dosimetry is well characterised and reproducible, no sample to sample measurement was undertaken.



Biological validation of hypoxia

The hypoxia inducible factor-1 α (HIF-1 α) is a well-known biomarker of hypoxia which is expressed upon hypoxia induction in human cells. Using immunofluorescent staining we detected HIF-1 α in human skin fibroblasts after hypoxia induction using our chambers. Briefly, the cells were incubated under the hypoxic gas mixture flow for 4 h and immediately fixed in 4% paraformaldehyde. Cells were then permeabilized, blocked in 10% goat serum and probed with a mouse primary anti-HIF-1 α antibody (Abcam, Cambridge, UK) and then washed and probed with goat-anti-mouse Alexa fluor 594 secondary antibody (ThermoFischer Scientific, UK). Finally, the cells were mounted with antifade reagent containing nuclear stain DAPI.

DNA DSB damage and repair under hypoxia

We detected DNA DSB damage and repair using the 53BP1 foci formation assay in hypoxic and oxic AG01522B cells irradiated with laser-driven protons, conventional protons and X-rays. Cells were gassed for four hours and then irradiated with 1 Gy of either 15 MeV laser-driven protons, conventional dose rate protons or X-rays. The cells were then fixed in 4% paraformaldehyde (PFA) for 20 min (room temperature) at 0.5- and 24-h post-irradiation. For co-staining with HIF-1 α and 53BP1, after fixation the samples were rinsed with PBS (Phosphate Buffered Saline) and later permeabilized in 0.5% Triton X-100 (Sigma Aldrich) in PBS for 10 min at room temperature and subsequently blocked in 2 ml of blocking buffer (10% goat serum and 0.25% Triton X-100 in PBS) at 37 °C for 2 h. After blocking, 1 ml of the primary antibodies mixture, 1:1000 53BP1 (Novus Biologicals, Littleton, CO, USA) and 1:500 HIF-1 α (Abcam, Cambridge, UK) diluted in the blocking medium was

added to the dishes and incubated at 37 °C for 1 h and then washed three times in PBS containing 0.1% Triton X-100. The cells were then probed with a mixture of secondary antibodies (goat anti-rabbit-Alexa Fluor 488 and goat anti-mouse-Alexa Fluor 594), at a dilution of 1:1000 respectively in blocking buffer and incubated for 1 h at 37 °C. The samples were then washed and mounted on coverslips using an anti-fade reagent containing DAPI. Cells were then scored for 53BP1 foci in both oxic and hypoxic samples and plotted as mean number of foci per cell for 0.5 and 24 h time points.

Oxygen enhancement ratio

We used the clonogenic cell survival assay to calculate the oxygen enhancement ratio for normal human skin fibroblasts (AG01522B) and patient derived radioresistant glioblastoma stem like cells (E2 Cells) irradiated with X-rays. As these two cell lines have variable intrinsic radiosensitivity, the X-ray dose response under hypoxia for these cell lines enabled further validation of the chambers' ability to maintain radiobiological hypoxia. Due to the technical difficulties involved in generating radiation doses in the range relevant for cell survival assay, it was not feasible to conduct cell survival assay with laser-accelerated protons during these studies and for this objective, we limited our experiments to X-rays only. Both the normal and radioresistant cells were plated at a density of 2×10^5 cells per dish on Mylar and incubated for 24 h. After 24 h, the cell culture medium was replaced with fresh medium and the dishes mounted inside hypoxia chambers connected to the hypoxia gas supply as described previously. After 4 h of gassing, the valves were closed, the chambers disconnected, and hypoxic cells exposed to various doses of X-rays. Immediately after irradiation, each chamber was opened, and the cells were dissociated and plated following the clonogenic assay protocol [37]. After twelve days we quantified the colonies in each well of the six-well plates, plotted dose response curves and calculated oxygen enhancement ratio at doses resulting in 10% (D_{10}), 50% (D_{50}) and 90% (D_{90}) surviving fraction for both cell lines to determine the impact of both low and high doses of X-rays, according to the formula

$$\text{OER} = D_{10,50 \text{ or } 90}(\text{Hypoxic}) / D_{10,50 \text{ or } 90}(\text{Oxic})$$

where $D_{10, 50 \text{ or } 90}$ = dose resulting in 10, 50 or 90% surviving fraction.

Data analysis and statistics

Oxygen measurements were carried out using six independent chambers and data is shown for individual chambers as well as the mean for six chambers for comparison. 53BP1 foci were analysed in at least

100 cells in three replicates and reported as mean values \pm standard error of the mean (SEM). Statistical significance analysis comparing the foci induction and cell survival values under oxic and hypoxic conditions was performed using an unpaired T test available in GraphPad Prism software, version 9.1.2 (LaJolla, CA, USA), with a threshold for significance at $P < 0.05$ and $P < 0.01$. For OER calculations, cell survival data from at least two independent X-rays dose response replicates in AG01522B and E2 cells were obtained and fitted in modified Linear Quadratic fitting of Graphpad Prism software. Various transformants reporting dose resulting in 10% cell survival (D_{10}), 50% cell survival (D_{50}) and 90% cell survival (D_{90}) were obtained from the fits with 95% confidential intervals (CI). The obtained values for D_{10} , D_{50} and D_{90} under hypoxia were divided with the D_{10} , D_{50} and D_{90} values obtained under normoxic conditions to obtain OER and shown as OER with 5% Error.

Results

Oxygen concentration measurement

We measured oxygen concentrations in six individual hypoxia chambers as shown in Fig. 3. All six chambers maintained a physiological hypoxic environment ($\leq 2\%$ O_2 [38]) for up to 4 h after disconnection from the gas supply. These chambers maintained radiobiological hypoxia ($\leq 0.4\%$ Oxygen [38]) for at least 45 min after disconnection from the gas supply, which provided sufficient time to irradiate and process the samples under radiobiological hypoxia conditions without the risk of re-oxygenation. When data for all chambers was fitted using a single curve, good agreement was found for the first six hours, where the oxygen concentrations remained below 2%. The best-fitting curve (line in Fig. 3) was in agreement with all chambers with a mean absolute deviation of 0.06% O_2 . The best-fitting parameters were $C_0 = 4.9 \pm 0.2\%$ O_2 and $k = 0.0012 \pm 0.0001 \text{ min}^{-1}$. For the early time period, this is equivalent to a reoxygenation rate of $0.00588 \pm 0.0005\%$ O_2/min . Chamber 3 showed some deviations from the rest of the chambers after 4 h of gassing. One significant outlier point was excluded from this analysis, for chamber 5 at 24 h, which showed an O_2 concentration of almost 7%, compared to 4% for the other chambers. This suggests there may be some greater variability at later time points, but that these chambers are suitable for maintaining radiobiological hypoxia over practical experimental timescales of at least 45 min which is sufficient to irradiate the cells while under radiobiological hypoxia and transport them back to the biology laboratory for further processing.

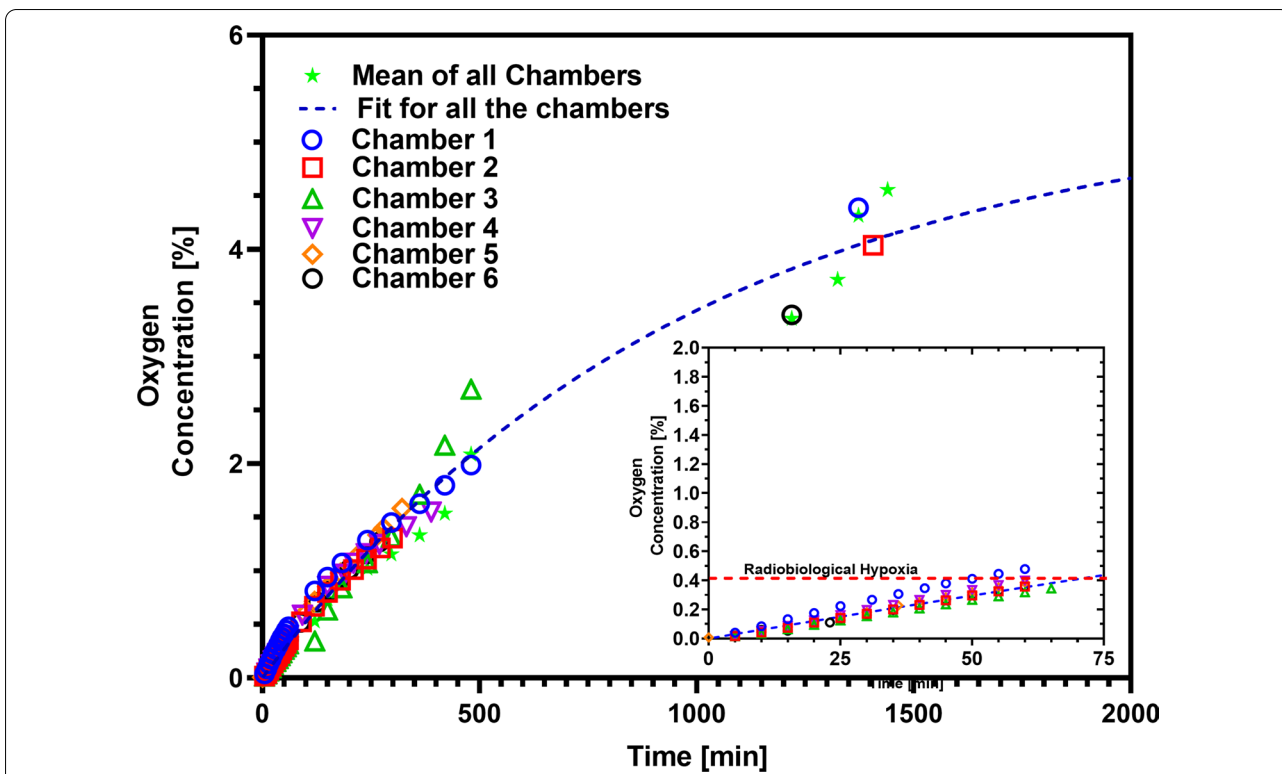


Fig. 3 Physical validation of hypoxia as carried out using an Oxygen sensing probe for measuring the Oxygen concentration measurement over the period of 24 h after gassing the six hypoxia chambers. The inset graphs shows the oxygen concentration during the first 75 min. For the initial 45 min after gassing, all the chambers maintained the oxygen level below 0.4% (radiobiological hypoxia shown by red-dashed line). The plot also shows the average of all chambers (bright green stars) and one phase association reoxygenation fitting is shown in blue dashed line. At later time points (24 h of gassing) some deviation in the oxygen concentration was also observed

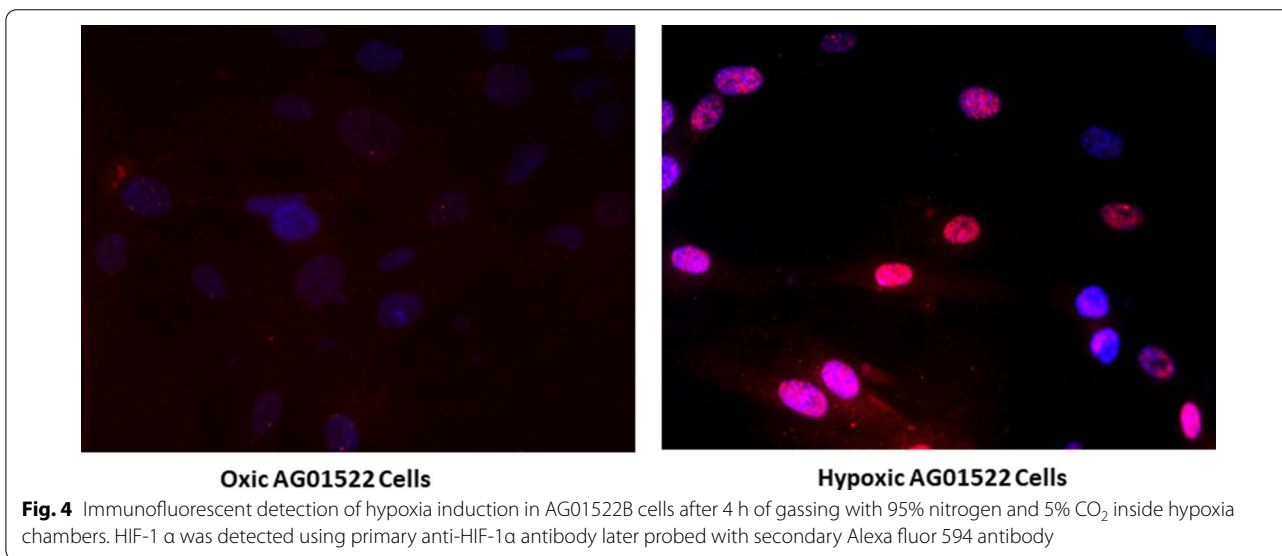


Fig. 4 Immunofluorescent detection of hypoxia induction in AG01522B cells after 4 h of gassing with 95% nitrogen and 5% CO₂ inside hypoxia chambers. HIF-1 α was detected using primary anti-HIF-1α antibody later probed with secondary Alexa fluor 594 antibody

Biological verification of hypoxia using HIF-1α

We used an immunofluorescent assay to detect HIF-1α in the AG01522B cells after 4 h hypoxia induction. As

shown in Fig. 4, HIF-1α is mainly localized in the nucleus of hypoxic cells while in the oxic samples only faint cytoplasmic staining is seen. We observed clear differences in

the intensity of HIF-1 α staining under both hypoxic and oxic conditions after four hours of gassing for hypoxia induction and similar changes were also noticed in the cells co-stained with DNA DSB marker 53BP1 and HIF-1 α .

DNA DSB damage induction and repair in hypoxic cells

53BP1 foci formation is regarded as one of the hallmarks of DNA DSB damage along with γ -H2AX [39–42]. We detected 53BP1 foci formation in AG01522B cells irradiated with 15 MeV laser-driven protons, conventional protons and X-rays with simultaneous staining of HIF-1 α as shown in Fig. 5a where the 53BP1 foci are shown in green, HIF-1 α in red and nucleus in blue. Quantitative analysis, as shown in Fig. 5b clearly indicates the effect of hypoxia on the DSB damage induction. Under oxic conditions, the levels of initial damage at 0.5 h induced by laser-driven protons, conventional protons and X-rays were similar, with mean 53BP1 foci per cell values of 24 ± 3 , 25.6 ± 3 and 24.9 ± 0.8 respectively. Similarly, under hypoxia, the levels of initial DNA DSB damage were similar for laser-driven protons, conventional dose rate protons and X-rays with mean 53BP1 foci levels of 14.16 ± 2.5 , 11.9 ± 1.5 and 10 ± 1 . Overall, a decrease in the mean 53BP1 foci per cell clearly show the impact of cellular hypoxia on the DNA DSB damage yields.

At 24 h post-irradiation, we detected significant changes ($P < 0.05$) in the mean number of residual 53BP1 foci induced by laser-driven protons under hypoxia with mean foci values of 4.5 ± 0.8 compared to mean values of 1.9 ± 0.5 and 1.8 ± 0.2 for conventional protons and

X-rays respectively. The residual foci measured for both conventional protons and X-rays were not significantly different from each other. We further compared the DSB foci induced by laser-driven protons and conventional protons by normalizing 53BP1 foci induction value at 0.5 and 24 h to those induced by X-rays defined as relative foci induction (RFI) as the ratio of foci induction by laser-driven or conventional proton to X-rays induced foci at same time point as shown in Additional file 1: Fig. S2. Laser-driven protons showed a statistically significant ($P < 0.05$) RFI value of 2.4 ± 0.2 compared to the conventional proton RFI value of 1.08 ± 0.1 for the residual (24 h) 53BP1 foci under hypoxia.

Oxygen enhancement ratio in AG01522B and patient-derived GBM stem cells

We calculated the oxygen enhancement ratio for cell survival of X-rays in both the normal AG01522B cells and E2 cells. Figure 6a shows the AG01522B cell survival curve for oxic and hypoxic conditions and Fig. 6b shows the cell survival curves for E2 cells under oxic and hypoxic conditions. Dose resulting in cell survival at various levels such as D_{10} , D_{50} and D_{90} were obtained for each cell line from the X-rays dose response curve under oxic and hypoxic conditions. The OER varied for each cell line and a dose dependent variation in OER was observed as shown in Additional file 1: Table S1. For normal human fibroblast cell line AG01522B cells we observed an OER value of 1.80 ± 0.09 , 2.0 ± 0.1 and 2.2 ± 0.1 respectively for D_{10} , D_{50} and D_{90} . For radioresistant E2 cells the OER values were 1.80 ± 0.09 , 2.2 ± 0.1 and 2.5 ± 0.1 . The OER values

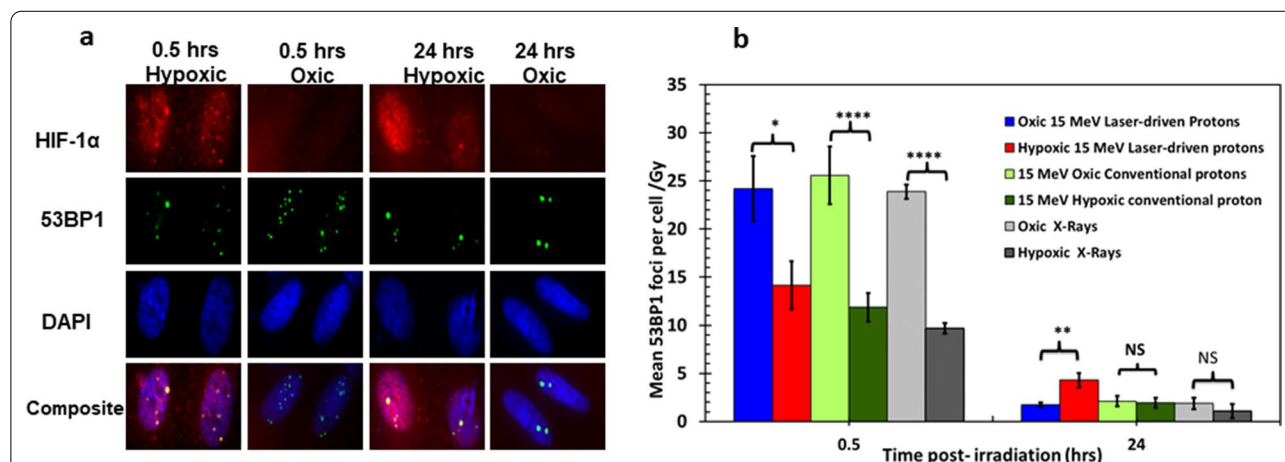
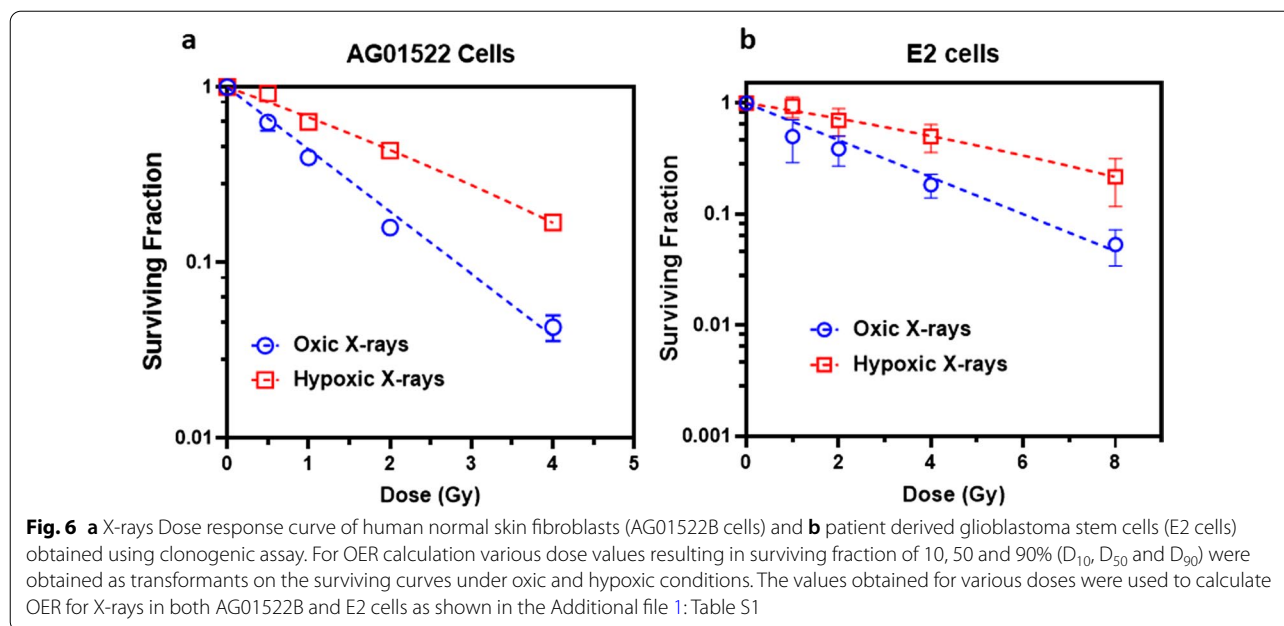


Fig. 5 **a** Laser accelerated 15 MeV protons induced DNA DSB damage and repair detection using 53BP1 foci formation assay in AG01522B cells irradiated under hypoxic and oxic conditions. Cells were incubated under hypoxia for 4 h, irradiated, then later fixed and stained for 53BP1 foci (green) and HIF-1 α (in red). **b** Quantification of laser -accelerated protons induced 53BP1 foci under oxic and hypoxic conditions for comparison cells in similar conditions were also irradiated with 1 Gy of 225 kVp X-rays. All the values on the graphs are shown after subtracting the background control values. For each data point at least 100 cells in duplicate slides were analyzed and data is shown as an average of two independent replicates. Error bars represent the standard error of the mean. Statistical significance was analysed using Student's un-paired *T* test and * represents P values ≤ 0.05 , *** represents P values ≤ 0.0001 ; NS-non-significant



varied both with the change in dose and the nature of cell lines. Variation in OER as a function of dose and cellular radiosensitivity are expected as also reported in [42, 43].

Discussion

Overcoming hypoxic radioresistance still remains one of the most important unmet challenges even with the most advanced radiotherapy modalities [44]. Despite the tremendous progress made in imaging hypoxia [45, 46] and radiotherapy modelling based concepts such as dose and LET painting with charged particles [5, 47, 48], the treatment of hypoxic tumours is still challenging. Radiobiological data on the effectiveness of charged particles under hypoxia is also still very limited. At UHDR above 10^7 Gy/s, only a few papers are available that show the role of oxygen depletion with electron beams [22] while there is no radiobiological data reported with UHDR protons. In this study, we successfully designed and developed compact portable hypoxia chambers and tested them for maintaining radiobiological hypoxia for extended periods after gassing and being disconnected from the gas supply. As laser-driven proton beam acceleration techniques are still evolving, cellular irradiation with laser-driven beams is not yet optimal in terms of—dose stability and the ability to raster scan at speed across a sample as possible with cyclotron accelerated proton beams. On the other hand, the achievement of UHDR exceeding 10^8 Gy/s in single pulses of \sim ns duration makes this an ideal approach to access and study novel radiobiological regimes.

Due to current constraints at high-power laser facilities, the time between irradiation of individual samples can vary from several minutes to an hour. Our hypoxia chambers facilitate the maintenance of hypoxia for the entire duration of transportation, alignment, irradiation and transport back to a biological laboratory for post-irradiation processing. Oxygen concentration values relevant to radiobiological, pathological and physiological levels of hypoxia and the hypoxia retention efficiency at all levels of the chambers are shown in Fig. 3. All six hypoxia chambers were able to maintain a physiological hypoxia environment ($\leq 2\%$ O_2) for the full 24 h test period and radiobiological hypoxia for about 45 min after disconnecting from the gas supply.

Hypoxia systems, currently in use, offer the capability of irradiating up to 6 samples simultaneously in a six-well plate format [31]. While this is advantageous to speed up the workflow, a possible downside is that, in case of any issue with the irradiation, all of the six samples are used. Our hypoxia chamber can be used to irradiate single samples one at a time, which minimizes the risk of sample wastage especially in case of laser-driven ions where the dose variation can be significant from sample to sample [49]. In addition, for multiple-sample hypoxia chambers, an accurate spatial sample translation system is required along with a higher sample irradiation rate. Both of these features are still not optimized for use with laser-driven ions, although these features are already used in practice with cyclotron-accelerated protons. For example on the LNS CATANA beam line, we have previously used a X- and Y-axis sample stage translator to

irradiate multiple fields on the same slide flask or several slide flasks in a short time fraction [37, 50, 51]. Some investigators have used an inflatable plastic bag [52, 53] to enclose the samples and keep them hypoxic, however this approach may not be suitable for applications where the samples are irradiated vertically, as in our case with laser driven ions. Also the geometry of the irradiation port and the safety guidelines may not allow the use of such inflatable chamber due to irregular shape and size and the risk that the bag punctures and contents spill out.

For reproducible dosimetry, a thin window membrane was used to minimise any impact of charged particle interactions within the chambers. We used GEANT4 simulation to verify energy and dose changes inside and outside the hypoxia chamber and found no changes as shown in Fig. 2f. Such dosimetry verifications are very important as the aluminium or other components used in chambers upon interaction with protons may lead to significant beam energy attenuation (particularly when working at moderate proton energies) or produce secondary particles, which may contribute to the delivered dose. In the previous studies, the investigators did not comment on whether the material of the chambers attenuated any dose or if there was any significant generation of the secondary particles upon the interaction of charged particles with hypoxia chamber materials [26, 31, 32].

Using the chambers, we tested the effects of hypoxia on key radiobiological endpoints such as DNA DSB damage and cell survival for two cell lines. We used AG01522B primary human fibroblasts as they have been extensively used as radiobiological models to represent normal cells [16, 17, 37, 51–54] and patient-derived glioblastoma E2 stem like cells, as a model system for radioresistant cells which have previously been used to evaluate the role of DNA damage signalling and DNA repair inhibitors in radiation-resistant brain tumours [55–57]. Due to the unavailability of the E2 cells at the time of the laser-driven experiments, we limited the DNA DSB damage assay to AG01522B cells, while for cell survival studies with X-rays we used both cell lines.

The main aim of this paper is to show the potential of the designed chamber to maintain radiobiological hypoxic environment during irradiations. Under normoxic conditions, only background cytoplasmic staining of HIF-1 α was observed while upon hypoxia induction for 4 h, an intense nuclear staining of HIF-1 α was clearly detected.

53BP1 foci formation is regarded as one of the hallmarks of DNA DSB damage [39–42, 58]. We detected 53BP1 foci formation in AG01522B cells irradiated with 15 MeV protons, with simultaneous staining of HIF-1 α , a hypoxia biomarker, by immunofluorescent microscopy as

shown in Fig. 5a. The images show the nuclear localisation of the 53BP1 foci in both the hypoxic and oxic samples. The initial DNA DSB damage yield as confirmed through 53BP1 foci at 0.5 h did not vary significantly among the cells irradiated with laser-driven protons, conventional dose rate protons or X-rays under normoxic conditions. This confirms other published data using γ -H2AX foci [15] and both γ -H2AX and 53BP1 [59] for 4.5 MeV [15] or 2.1 MeV [59] laser-driven protons, X-rays or cyclotron-accelerated protons under normoxia. In our study, for the first time we also compare laser-driven proton effects at ultra-high dose-rate under oxic and hypoxic conditions and show that residual DNA DSB damage at 24 h post-irradiation was significantly higher ($P < 0.05$) in hypoxic cells compared to the oxic AG01522B cells. In contrast, the residual DNA DSB damage levels induced by X-rays and conventional dose rate protons, both under the normoxic and hypoxic conditions were similar. So far, at lower dose-rates, (~ 100 Gy/s) studies of FLASH effects have observed these mainly under in vivo conditions [20, 21, 60–63] and only a few investigators have studied them under in vitro conditions [22, 64, 65]. While the normal tissue sparing effects of FLASH irradiation are unique, still no clear mechanisms have been identified for the observed effects. Ultra-high dose rate induced oxygen depletion was hypothesized several decades ago [18] and several investigators have recently observed FLASH effects under reduced oxygen conditions or hypoxia e.g. prostate cancer cells when irradiated at FLASH dose rates under hypoxia [22] showed a higher surviving fractions compared to similar doses at conventional dose rates. Furthermore, upon increasing the oxygen concentration during FLASH irradiation, Montay Gruel et al. observed that the sparing of the neurocognitive functions in mice decreased [9] after irradiation, indicating that a reduced oxygen concentration during irradiation at FLASH dose rates favours tissue sparing.

Recent modelling studies have tested the role of FLASH irradiation-induced oxygen depletion [23, 24, 66–68] and suggest that the radiation doses required to induce radiobiological hypoxia are several magnitudes higher than the dose used for in vivo and in vitro FLASH experiments. However, the model of radiation induced transient oxygen depletion, as suggested by Favaudon et al., seems to be a reasonable explanation for the FLASH effects alongside the differential nature and variations in the bimolecular composition, metabolism, free radicals generation and free radicals clearance mechanisms of the normal and cancer cells [69].

Similar amount of cell killing and DNA DSB damage with electrons at FLASH and conventional dose rates have been observed in cancer and normal cells, as suggested earlier under oxic conditions. In contrast,

the higher residual DNA DSB damage under hypoxia observed here with laser-driven protons at ultra-high dose-rates clearly suggests a dose rate effect, which has not so far been reported. As residual DNA DSB damage observed through persistent γ -H2AX foci has been associated with late normal tissue toxicity [70], it is reasonable to infer that the higher residual 53BP1 foci levels measured under hypoxia may result in enhanced cell killing. Enhanced cell killing under hypoxia would clearly lead to improved tumour control as hypoxia is a prominent feature of solid tumours [71] in contrast to normal tissues which may become transiently hypoxic during the irradiation (due to local oxygen depletion if the dose/dose-rate is high enough). This warrants further investigation and confirmation of the yields of DNA DSB damage induced by laser-driven proton under hypoxia, and, for a more comprehensive assessment of the effect, future studies should include comparisons in a wider range of models.

As DNA DSB damage is a key mediator of cell-death, we also tested whether the hypoxic environment inside the chambers has any impact on cell survival. OER is a widely used parameter [27, 72] under both clinical and pre-clinical settings to quantify oxygen sensitisation [73, 74]. We quantified the OER for cell survival of the AG01522B and patient derived E2 GBM stem cells following X-rays irradiation. As shown in Fig. 6a and b the dose response curve of the two cell lines differs due to their intrinsic radiosensitivity. The OER value for the AG01522B cells was 2.2 ± 0.1 , lower than that measured for the radioresistant E2 cells (2.5 ± 0.1) at D_{90} similar to the OER values reported for various normal and tumour cell lines [75, 76].

Our hypoxia chambers, once gassed, can be used as a standalone unit unlike the previously developed systems, which rely on continuous gassing [31], and can result in a bulky system. Thanks to their portability and bespoke design, the chambers enabled the first radiobiology measurements under controlled oxygen conditions employing laser driven protons, as well as allowing comparator measurements employing conventional dose rate protons and X-rays.

Conclusions

In this manuscript, we have described the development of a portable hypoxia chamber specifically designed for use in radiobiology experiments in ultra-high dose rates regimes employing beams of laser-driven protons. We have also presented the chamber's successful application to the study of radiobiological endpoints such as DNA DSB damage and cell survival employing not only laser-driven protons, but also conventional proton and X-ray sources for reference studies. Our results indicate

similarities with previously published data but also provide a novel benchmark indicating higher residual DNA DSB damage inflicted by laser-driven UHDR protons under hypoxia compared to cyclotron-accelerated protons.

Supplementary Information

The online version contains supplementary material available at <https://doi.org/10.1186/s13014-022-02024-3>.

Additional file 1. Supplementary tables and figures.

Acknowledgements

The authors are thankful to Prof. Stanley W. Botchway (Research Complex at Harwell), Chantal Fowler (Central Laser Facility), Sarah Grattan (Research Complex at Harwell) for providing access and support in Biology laboratory. We also acknowledge support of Stephen Barnard and Graham Holliman (Public Health England) for providing access to X-rays source. Furthermore, we are thankful to the workshop staff of Queen's University Belfast and the Central Laser Facility. We sincerely thank Prof Anthony Chalmers and Prof. Colin Watts for providing patient-derived GBM stem cells.

Authors' contributions

PC, MB, KMP conceptualized the study. MB, KMP and PMcK wrote the project. PC, DG and DD designed the hypoxia chambers. PC, DG, BO, AM and CM performed physical and biological measurements, analysed the data. PC, DG, MB and KMP wrote the manuscript. DD, HA, LR, AA, HP, GM and SK set-up the experiment, and generated and characterized the laser-driven protons. GM carried out Monte Carlo simulations and obtained various parameters. SJM helped with OER calculation fittings in Prizm software. JG, NB and DC facilitated and supported the experiments in Rutherford Appleton Laboratory and GP, RC, FPC and GAP, provided the facility and supported experiments with cyclotron-accelerated protons. All authors read and approved the final manuscript.

Funding

Authors acknowledge the funding received from the Engineering and Physical Sciences Research Council (EPSRC), through Grants EP/K022415/1, EP/J500094/1 and EP/P010059/1. This work has also been partly supported by project 18HLT04 UHD pulse, which has received funding from the EMPIR programme co-financed by the Participating States and from the European Union's Horizon 2020 Research and Innovation Programme. Additionally, Boris Odlozilik acknowledges funding from the European Union's Horizon 2020 research and innovation program under the Marie Skłodowska-Curie grant agreement no 754507. KMP acknowledges support from Brainwaves NI. Aaron McMurray acknowledges the funding support provided by Department for the Economy, Northern Ireland.

Availability of data and materials

Raw data can be available upon request from the Corresponding authors.

Declarations

Ethics approval and consent to participate

Not applicable.

Consent for publication

Not applicable.

Competing interests

The authors declare no competing financial and non-financial interests.

Author details

¹The Patrick G. Johnston Centre for Cancer Research, Queen's University Belfast, Lisburn Road, Belfast BT9 7AE, Northern Ireland, UK. ²Centre for Plasma Physics, School of Mathematics and Physics, Queen's University Belfast,

Belfast BT7 1NN, Northern Ireland, UK. ³Extreme Light Infrastructure (ELI-NP) and Horia Hulubei National Institute for R & D in Physics and Nuclear Engineering (IFIN-HH), Str. Reactorului No. 30, 077125 Bucharest, Magurele, Romania. ⁴Laboratoire LULI, École Polytechnique, Route de Saclay, 91128 Palaiseau, Paris, France. ⁵Experimental Science Group, Central Laser Facility, Rutherford Appleton Laboratory, Didcot, Oxford OX11 0QX, England, UK. ⁶Department of Physics, SUPA, University of Strathclyde, Glasgow G1 1XQ, Scotland, UK. ⁷Laboratori Nazionali del Sud - Istituto Nazionale di Fisica Nucleare, Via S. Sofia 62, 95123 Catania, Italy. ⁸ELI-Beamlines Centre, Institute of Physics, Czech Academy of Sciences, Za Radnicí 835, 252 41 Dolní Břežany, Czech Republic.

Received: 29 June 2021 Accepted: 3 March 2022
Published online: 15 April 2022

References

- Gray LH, Conger AD, Ebert M, Hornsey S, Scott OC. The concentration of oxygen dissolved in tissues at the time of irradiation as a factor in radiotherapy. *Br J Radiol.* 1953;26(312):638–48. <https://doi.org/10.1259/0007-1285-26-312-638>.
- Barendsen GW. Responses of cultured cells, tumours and normal tissues to radiations of different linear energy transfer. *Curr Top Radiat Res Vol IV* Ebert, Michael Howard, Alma (eds) New York, John Wiley Sons, Inc; 1968. pp. 293–356. Available from: <https://www.osti.gov/biblio/4500126>.
- Prise KM, Folkard M, Davies S, Michael BD. The irradiation of V79 mammalian cells by protons with energies below 2 MeV. Part II. Measurement of oxygen enhancement ratios and DNA damage. *Int J Radiat Biol.* 1990;58(2):261–77. <https://doi.org/10.1080/09553009014551611>.
- Nakano T, Suzuki Y, Ohno T, Kato S, Suzuki M, Morita S, et al. Carbon beam therapy overcomes the radiation resistance of uterine cervical cancer originating from hypoxia. *Clin Cancer Res.* 2006;12:2185–90. <https://doi.org/10.1158/1078-0432.CCR-05-1907>.
- Bassler N, Jäkel O, Søndergaard CS, Petersen JB. Dose- and LET-painting with particle therapy. *Acta Oncol.* 2010;49(July):1170–6. <https://doi.org/10.3109/0284186X.2010.510640>.
- Hirayama R, Furusawa Y, Fukawa T, Ando K. Repair kinetics of DNA-DSB induced by X-rays or carbon ions under oxic and hypoxic conditions. *J Radiat Res.* 2005;46(3):325–32. <https://doi.org/10.1269/jrr.46.325>.
- Mohan R, Grosshans D. Proton therapy: present and future. *Adv Drug Deliv Rev.* 2017;109:26–44. <https://doi.org/10.1016/j.addr.2016.11.006>.
- Fowler JF. What can we expect from dose escalation using proton beams? *Clin Oncol.* 2003;15(1):10–5. <https://doi.org/10.1053/clon.2002.0182>.
- Montay-Gruel P, Acharya MM, Petersson K, Alikhani L, Yakkala C, Allen BD, et al. Long-term neurocognitive benefits of FLASH radiotherapy driven by reduced reactive oxygen species. *Proc Natl Acad Sci USA.* 2019;166(22):10943–51. <https://doi.org/10.1073/pnas.1901777116>.
- Montay-Gruel P, Meziani L, Yakkala C, Vozenin MC. Expanding the therapeutic index of radiation therapy by normal tissue protection. *Br J Radiol.* 2019. <https://doi.org/10.1259/bjr.20180008>.
- Diffenderfer ES, Verginadis II, Kim MM, Shoniyozov K, Velapoulou A, Goia D, et al. Design, implementation, and in vivo validation of a novel proton FLASH radiation therapy system. *Int J Radiat Oncol Biol Phys.* 2020;106(2):440–8. <https://doi.org/10.1016/j.ijrobp.2019.10.049>.
- Doria D, Kakolee KF, Kar S, Litt SK, Fiorini F, Ahmed H, et al. Biological effectiveness on live cells of laser driven protons at dose rates exceeding 109 Gy/s. *AIP Adv.* 2012;2(1):011209. <https://doi.org/10.1063/1.3699063>.
- Yogo A, Maeda T, Hori T, Sakaki H, Ogura K, Nishiuchi M, et al. Measurement of relative biological effectiveness of protons in human cancer cells using a laser-driven quasimonoeenergetic proton beamline. *Appl Phys Lett.* 2011;98(5):053701. <https://doi.org/10.1063/1.3551623>.
- Zeil K, Baumann M, Beyreuther E, Burris-Mog T, Cowan TE, Enghardt W, et al. Dose-controlled irradiation of cancer cells with laser-accelerated proton pulses. *Appl Phys B Lasers Opt.* 2013;110(4):437–44. <https://doi.org/10.1007/s00340-012-5275-3.pdf>.
- Bin J, Allinger K, Assmann W, Dollinger G, Drexler GA, Friedl AA, et al. A laser-driven nanosecond proton source for radiobiological studies. *Appl Phys Lett.* 2012;110:437–44. <https://doi.org/10.1007/s00340-012-5275-3>.
- Hanton F, Chaudhary P, Doria D, Gwynne D, Maiorino C, Scullion C, et al. DNA DSB repair dynamics following irradiation with laser-driven protons at ultra-high dose rates. *Sci Rep.* 2019. <https://doi.org/10.1038/s41598-019-40339-6>.
- Manti L, Perozziello FM, Borghesi M, Candiano G, Chaudhary P, Cirrone GAP, et al. The radiobiology of laser-driven particle beams: focus on sub-lethal responses of normal human cells. *J Instrum.* 2017;12(03):C03084.
- Weiss H, Epp ER, Heslin JM, Ling CC, Santomasso A. Oxygen depletion in cells irradiated at ultra-high dose-rates and at conventional dose-rates. *Int J Radiat Biol Relat Stud Physics, Chem Med.* 1974;26(1):17–29. <https://doi.org/10.1080/09553007414550901>.
- Durante M, Brauer-Krisch E, Hill M. Faster and safer? FLASH ultra-high dose rate in radiotherapy. *Br J Radiol.* 2017. <https://doi.org/10.1259/bjr.20170628>.
- Favaudon V, Caplier L, Monceau V, Pouzoulet F, Sayarath M, Fouillade C, et al. Ultrahigh dose-rate FLASH irradiation increases the differential response between normal and tumor tissue in mice. *Sci Transl Med.* 2014;6(245):1–10. <https://doi.org/10.1126/scitranslmed.3008973>.
- Montay-Gruel P, Petersson K, Jaccard M, Boivin G, Germond JF, Petit B, et al. Irradiation in a flash: unique sparing of memory in mice after whole brain irradiation with dose rates above 100 Gy/s. *Radiother Oncol.* 2016;124(3):365–9. <https://doi.org/10.1016/j.radonc.2017.05.003>.
- Adrian G, Konradsson E, Lempart M, Bäck S, Ceberg C, Petersson K. The FLASH effect depends on oxygen concentration. *Br J Radiol.* 2020;93(1106):20190702. <https://doi.org/10.1259/bjr.20190702>.
- Petersson K, Adrian G, Butterworth K, McMahon SJ. A quantitative analysis of the role of oxygen tension in FLASH radiation therapy. *Int J Radiat Oncol Biol Phys.* 2020;107(3):539–47. <https://doi.org/10.1016/j.ijrobp.2020.02.634>.
- Khan S, Bassenne M, Wang J, Manjappa R, Melemenidis S, Breikreutz DY, et al. Multicellular spheroids as in vitro models of oxygen depletion during FLASH irradiation. *Int J Radiat Oncol.* 2021;110:833–44. <https://doi.org/10.1016/j.ijrobp.2021.01.050>.
- Lee KB, Kim K-R, Huh T-L, Lee YM. Proton induces apoptosis of hypoxic tumor cells by the p53-dependent and p38/JNK MAPK signalling pathways. *Int J Oncol.* 2008;33:1247–56. https://doi.org/10.3892/ijo_00000115.
- Ma NY, Tinganelli W, Maier A, Durante M, Kraft-Weyrather W. Influence of chronic hypoxia and radiation quality on cell survival. *J Radiat Res.* 2013;54:13–22. <https://doi.org/10.1093/jrr/rrs135>.
- Tinganelli W, Durante M, Hirayama R, Krämer M, Maier A, Kraft-Weyrather W, et al. Kill-painting of hypoxic tumours in charged particle therapy. *Sci Rep.* 2015;5:1–13. <https://doi.org/10.1038/srep17016>.
- Kanemoto A, Hirayama R, Moritake T, Furusawa Y, Sun L, Sakae T, et al. RBE and OER within the spread-out Bragg peak for proton beam therapy: in vitro study at the Proton Medical Research Center at the University of Tsukuba. *J Radiat Res.* 2014;55(5):1028–32. <https://doi.org/10.1093/jrr/rru043>.
- Kumareswaran R, Ludkovski O, Meng A, Sykes J, Pintilie M, Bristow RG. Chronic hypoxia compromises repair of DNA double-strand breaks to drive genetic instability. *J Cell Sci.* 2012;125:189–99. <https://doi.org/10.1242/jcs.092262>.
- Vordermark D, Menke DR, Brown JM, Ma N-Y-N-Y, Tinganelli W, Maier A, et al. Similar radiation sensitivities of acutely and chronically hypoxic cells in HT 1080 Fibrosarcoma Xenografts. *Nat Rev Cancer.* 2013;4(1):443–7. <https://doi.org/10.1016/j.jscs.2010.02.005>.
- Metsälä O, Kreutzer J, Högel H, Miiikkulainen P, Kallio P, Jaakkola PM. Transportable system enabling multiple irradiation studies under simultaneous hypoxia in vitro. *Radiat Oncol.* 2018;13(1):220. <https://doi.org/10.1186/s13014-018-1169-9>.
- Tinganelli W, Ma NY, Von Neubeck C, Maier A, Schicker C, Kraft-Weyrather W, et al. Influence of acute hypoxia and radiation quality on cell survival. *J Radiat Res.* 2013;54(Suppl 1):23–30. <https://doi.org/10.1093/jrr/rrt065>.
- Snavely RA, Key MH, Hatchett SP, Cowan TE, Roth M, Phillips TW, et al. Intense high-energy proton beams from Petawatt-laser irradiation of solids. *Phys Rev Lett.* 2000;85(14):2945–8.
- Macchi A, Borghesi M, Passoni M. Ion acceleration by superintense laser-plasma interaction. *Rev Mod Phys.* 2013;85(2):751–93. <https://doi.org/10.1103/RevModPhys.85.751>.
- Karsch L, Beyreuther E, Burris-Mog T, Kraft S, Richter C, Zeil K, et al. Dose rate dependence for different dosimeters and detectors: TLD, OSL, EBT films, and diamond detectors. *Med Phys.* 2012;39(5):2447–55. <https://doi.org/10.1118/1.3700400>.

36. Jaccard M, Petersson K, Buchillier T, Germond JF, Durán MT, Vozenin MC, et al. High dose-per-pulse electron beam dosimetry: Usability and dose-rate independence of EBT3 Gafchromic films: Usability. *Med Phys*. 2017;44(2):725–35. <https://doi.org/10.1002/mp.12066>.
37. Chaudhary P, Marshall TI, Perozziello FM, Manti L, Currell FJ, Hanton F, et al. Relative biological effectiveness variation along monoenergetic and modulated Bragg peaks of a 62-MeV therapeutic proton beam: a preclinical assessment. *Int J Radiat Oncol Biol Phys*. 2014;90(1):27–35. <https://doi.org/10.1016/j.ijrobp.2014.05.010>.
38. McKeown SR. Defining normoxia, physoxia and hypoxia in tumours-implications for treatment response. *Br J Radiol*. 2013;2014(87):20130676. <https://doi.org/10.1259/bjr.20130676>.
39. Neumaier T, Swenson J, Pham C, Polyzos A, Lo AT, Yang P, et al. From the cover: evidence for formation of DNA repair centers and dose-response nonlinearity in human cells. *Proc Natl Acad Sci*. 2012;109(2):443–8. <https://doi.org/10.1073/pnas.1117849108>.
40. Asaithamby A, Chen DJ. Cellular responses to DNA double-strand breaks after low-dose gamma-irradiation. *Nucleic Acids Res*. 2009;37(12):3912–23.
41. Panier S, Boulton SJ. Double-strand break repair: 53BP1 comes into focus. *Nat Rev Mol Cell Biol*. 2014;15(1):7–18.
42. Zimmermann M, de Lange T. 53BP1: pro choice in DNA repair. *Trends Cell Biol*. 2014;24(2):108–17.
43. Freyer JP, Jarrett K, Carpenter S, Raju MR. Oxygen enhancement ratio as a function of dose and cell cycle phase for radiation-resistant and sensitive CHO cells. *Radiat Res*. 1991;127(3):297–307. <https://doi.org/10.2307/3577945>.
44. Wenzl T, Wilkens JJ. Theoretical analysis of the dose dependence of the oxygen enhancement ratio and its relevance for clinical applications. *Radiat Oncol*. 2011;6(1):1–9.
45. Burroughs SK, Kaluz S, Wang D, Wang K, Meir EG Van, Wang B. *Therapeutics*. 2014;5(5):1–31. <https://doi.org/10.4155/fmc.13.17>
46. Busk M, Overgaard J, Horsman MR. Imaging of tumor hypoxia for radiotherapy: current status and future directions. *Semin Nucl Med*. 2020;50(6):562–83. <https://doi.org/10.1053/j.semnuclmed.2020.05.003>.
47. Malinen E, Sövik Å. Dose or LET painting: What is optimal in particle therapy of hypoxic tumors? *Acta Oncol (Madr)*. 2015;54(9):1614–22. <https://doi.org/10.3109/0284186X.2015.1062540>.
48. Chang JH, Wada M, Anderson NJ, Lim Joon D, Lee ST, Gong SJ, et al. Hypoxia-targeted radiotherapy dose painting for head and neck cancer using (18) F-FMISO PET: a biological modeling study. *Acta Oncol*. 2012;2013(52):1723–9.
49. Romano F, Subiel A, McManus M, Lee ND, Palmans H, Thomas R, et al. Challenges in dosimetry of particle beams with ultra-high pulse dose rates. *J Phys Conf Ser*. 2020;1662(1):5. <https://doi.org/10.1088/1742-6596/1662/1/012028>.
50. Bravatà V, Tinganelli W, Cammarata FP, Minafra L, Calvaruso M, Sokol O, et al. Hypoxia transcriptomic modifications induced by proton irradiation in u87 glioblastoma multiforme cell line. *J Pers Med*. 2021;11(4):308. <https://doi.org/10.3390/jpm11040308>.
51. Chaudhary P, Marshall TI, Currell FJ, Kacperek A, Schettino G, Prise KM. Variations in the processing of DNA double-strand breaks along 60-MeV therapeutic proton beams. *Int J Radiat Oncol Biol Phys*. 2016;95(1):86–94. <https://doi.org/10.1016/j.ijrobp.2015.07.2279>.
52. Wang R, Jin F, Zhong H. A novel experimental hypoxia chamber for cell culture. *Am J Cancer Res*. 2014;4(1):53–60.
53. Kaida A, Miura M. Differential dependence on oxygen tension during the maturation process between monomeric Kusabira Orange 2 and monomeric Azami Green expressed in HeLa cells. *Biochem Biophys Res Commun*. 2012;421(4):855–9. <https://doi.org/10.1016/j.bbrc.2012.04.102>.
54. Marshall TI, Chaudhary P, Michaelidesová A, Vachelová J, Davidková M, Vondráček V, et al. Investigating the implications of a variable RBE on proton dose fractionation across a clinical pencil beam scanned spread-out Bragg peak. *Int J Radiat Oncol Biol Phys*. 2016;95(1):70–7. <https://doi.org/10.1016/j.ijrobp.2016.02.029>.
55. Gomez-Roman N, Stevenson K, Gilmour L, Hamilton G, Chalmers AJ. A novel 3D human glioblastoma cell culture system for modeling drug and radiation responses. *Neuro Oncol*. 2017;19(2):229–41. <https://doi.org/10.1093/neuonc/nw164>.
56. Ahmed U, Carruthers R, Gilmour L, Yildirim S, Watts C, Chalmers AJ. Selective inhibition of parallel DNA damage response pathways optimizes radiosensitization of glioblastoma stem-like cells. *Cancer Res*. 2015;75(21):4416–28. <https://doi.org/10.1158/0008-5472.CAN-14-3790>.
57. Carruthers R, Ahmed SU, Strathdee K, Gomez-Roman N, Amoah-Buahin E, Watts C, et al. Abrogation of radioresistance in glioblastoma stem-like cells by inhibition of ATM kinase. *Mol Oncol*. 2015;9(1):192–203. <https://doi.org/10.1016/j.molonc.2014.08.003>.
58. Asaithamby A, Hu B, Chen DJ. Unrepaired clustered DNA lesions induce chromosome breakage in human cells. *Proc Natl Acad Sci USA*. 2011;108(20):8293–8.
59. Raschke S, Spickermann S, Toncian T, Swantusch M, Boeker J, Giesen U, et al. Ultra-short laser-accelerated proton pulses have similar DNA-damaging effectiveness but produce less immediate nitroxidative stress than conventional proton beams. *Sci Rep*. 2016;6(1):32441.
60. Vozenin MC, De Fornel P, Petersson K, Favaudon V, Jaccard M, Germond JF, et al. The advantage of FLASH radiotherapy confirmed in mini-pig and cat-cancer patients. *Clin Cancer Res*. 2019;25(1):35–42. <https://doi.org/10.1158/1078-0432.CCR-17-3375>.
61. Alaghband Y, Cheeks SN, Allen BD, Montay-Gruel P, Doan NL, Petit B, et al. Neuroprotection of radiosensitive juvenile mice by ultra-high dose rate flash irradiation. *Cancers (Basel)*. 2020;12(6):1–21. <https://doi.org/10.3390/cancers12061671>.
62. Bourhis J, Sozzi WJ, Jorge PG, Gaide O, Bailat C, Duclos F, et al. Treatment of a first patient with FLASH-radiotherapy. *Radiother Oncol*. 2019;139:18–22. <https://doi.org/10.1016/j.radonc.2019.06.019>.
63. Favaudon V, Caplier L, Monceau V, Pouzoulet F, Sayarath M, Fouillade C, et al. Ultrahigh dose-rate FLASH irradiation increases the differential response between normal and tumor tissue in mice. *Sci Transl Med*. 2014;6(245):245ra93.
64. Buonanno M, Griji V, Brenner DJ. Biological effects in normal cells exposed to FLASH dose rate protons. *Radiother Oncol*. 2019;139:51–5. <https://doi.org/10.1016/j.radonc.2019.02.009>.
65. Adrian G, Konradsson E, Beyer S, Wittrup A, Butterworth KT, McMahon SJ, et al. Cancer cells can exhibit a sparing FLASH effect at low doses under normoxic in vitro-conditions. *Front Oncol*. 2021;11(July):1–9. <https://doi.org/10.3389/fonc.2021.686142>.
66. Boscolo D, Scifoni E, Durante M, Krämer M, Fuss MC. May oxygen depletion explain the FLASH effect? A chemical track structure analysis. *Radiother Oncol*. 2021;162:68–75. <https://doi.org/10.1016/j.radonc.2021.06.031>.
67. Jansen J, Knoll J, Beyreuther E, Pawelke J, Skuza R, Hanley R, et al. Does FLASH deplete oxygen? Experimental evaluation for photons, protons, and carbon ions. *Med Phys*. 2021;48(7):3982–90. <https://doi.org/10.1002/mp.14917>.
68. Abolfath R, Grosshans D, Mohan R. Oxygen depletion in FLASH ultra-high-dose-rate radiotherapy: a molecular dynamics simulation. *Med Phys*. 2020;47(12):6551–61. <https://doi.org/10.1002/mp.14548>.
69. Favaudon V, Labarbe R, Limoli CL. Model studies of the role of oxygen in the FLASH effect. *Med Phys*. 2021. <https://doi.org/10.1002/mp.15129>.
70. Bourton EC, Plowman PN, Smith D, Arlett CF, Parris CN. Prolonged expression of the γ -H2AX DNA repair biomarker correlates with excess acute and chronic toxicity from radiotherapy treatment. *Int J Cancer*. 2011;129(12):2928–34.
71. Najafi M, Farhood B, Mortezaee K, Kharazinejad E, Majidpoor J, Ahadi R. Hypoxia in solid tumors: a key promoter of cancer stem cell (CSC) resistance. *J Cancer Res Clin Oncol*. 2020;146(1):19–31. <https://doi.org/10.1007/s00432-019-03080-1>.
72. Antonovic L, Lindblom E, Dasu A, Bassler N, Furusawa Y, Toma-Dasu I. Clinical oxygen enhancement ratio of tumors in carbon ion radiotherapy: the influence of local oxygenation changes. *J Radiat Res*. 2014;55:902–11.
73. Thompson HF, Butterworth KT, McMahon SJ, Ghita M, Hounsell AR, Prise KM. The impact of hypoxia on out-of-field cell survival after exposure to modulated radiation fields. *Radiat Res*. 2017;188(6):716–24. <https://doi.org/10.1667/RR14836.1>.
74. Butterworth KT, McGarry CK, Clasie B, Carabe-Fernandez A, Schuemann J, Depauw N, et al. Relative biological effectiveness (RBE) and out-of-field cell survival responses to passive scattering and pencil beam scanning proton beam deliveries. *Phys Med Biol*. 2012;57(20):6671–80.
75. Wenzl T, Wilkens JJ. Modelling of the oxygen enhancement ratio for ion beam radiation therapy. *Phys Med Biol*. 2011;56(11):3251–68. <https://doi.org/10.1088/0031-9155/56/11/006>.
76. Chan CC, Chen FH, Hsiao YY. Impact of hypoxia on relative biological effectiveness and oxygen enhancement ratio for a 62-mev therapeutic proton beam. *Cancers (Basel)*. 2021;13(12):1–18. <https://doi.org/10.3390/cancers13122997>.

Publisher's Note

Springer Nature remains neutral with regard to jurisdictional claims in published maps and institutional affiliations.